HHS Public Access

Author manuscript

Breast Imaging (2012). Author manuscript; available in PMC 2017 August 21.

Published in final edited form as:

Breast Imaging (2012). 2012 July ; 7361: 300–307. doi:10.1007/978-3-642-31271-7_39.

The Impact of Reduced Injected Radioactivity on Image Quality of Molecular Breast Imaging Tomosynthesis

Olivia Sullivan[1], **Zongyi Gong**[1], **Kelly Klanian**[2], **Tushita Patel**[1], and **Mark B. Williams**[1,2,3]

[1]University of Virginia Department of Physics, Charlottesville, Virginia, USA

[2]University of Virginia Department of Biomedical Engineering Charlottesville, Virginia, USA

[3]University of Virginia Department of Radiology and Medical Imaging, Charlottesville, Virginia, USA

Abstract

This study's objective is to compare image quality in 3-D molecular breast imaging tomosynthesis (MBIT) with that in planar molecular breast imaging (MBI) over a range of breast radioactivity concentrations. Using gelatin and point source phantoms lesion contrast, lesion signal-to-noise ratio (SNR) and spatial resolution were compared for a range of lesion sizes and depths. For both MBI and MBIT, lesion contrast is essentially constant with changing activity while SNR decreases by a factor of 1.5 – 2 between 100% and 25% activity levels. For nearly all lesion sizes and locations contrast and SNR are significantly higher for MBIT than MBI, potentially permitting greater reductions in injected dose. Spatial resolution in MBI is dependent on lesion depth but independent of lesion location with MBIT. Reconstructed MBIT spatial resolution is substantially better than that in the projection images, suggesting future use of higher sensitivity collimators for even further reductions in injected activity.

Keywords

tomosynthesis; molecular breast imaging; radiation dose

1 Introduction

Breast cancer is one of the most commonly diagnosed cancers among US women. In 2011, an estimated 230,480 new cases of invasive and 57,650 cases of non-invasive (in situ) breast cancer are expected to be diagnosed [1]. Nevertheless, breast cancer death rates have been steadily declining since 1991 and this is thought to be partially a result of earlier detection through screening.

The current gold standard for breast cancer screening is x-ray mammography. However, the sensitivity of mammography is significantly reduced among the 40 – 60 % of women with radiodense breasts. The recent advent of x-ray tomosynthesis, in which multiple views of the breast are taken at different angles and then combined to form a 3-dimensional image, has shown promise for reducing the masking effect of radiodense breast tissue by providing some resolution along the direction of breast compression.

At the same time, new imaging modalities are being investigated as functional imaging adjuncts to the anatomical images of x-ray mammography and x-ray tomosynthesis. Breast scintigraphy using small field of view, dedicated breast gamma cameras and the radiopharmaceutical ^{99m}Tc-sestamibi, referred to as Molecular Breast Imaging (MBI) or Breast Specific Gamma Imaging (BSGI), is a relatively new functional imaging modality and has entered clinical practice. Although MBI provides functional information complementary to the anatomical information of mammography [3][5], with currently recommended tracer injected activity (740 – 1110 MBq) it results in an effective whole body radiation dose of ~6 – 9 mSv. Although the additional radiation dose to the breast from MBI is comparable to that of a single mammographic view, other organs also receive dose, resulting in the larger effective dose for MBI compared to screening mammography (0.7–1.0 mSv)[5]. While this dose is comparable to that of many nuclear medicine scans, it may be more than is necessary for good quality MBI, especially given the improving imaging technologies becoming available. Thus efforts are underway to investigate the impact on MBI image quality of lowering the amount of injected radiotracer [4].

Our group is developing a dual modality tomosynthesis (DMT) scanner in which x-ray breast tomosynthesis (XBT) and molecular breast imaging tomosynthesis (MBIT) images are obtained with the breast in a single configuration under mild compression. Like XBT, in MBIT multiple gamma emission views are obtained over a range of viewing angles. Both modalities are mounted on a common upright mammography-style gantry. Following XBT the gamma camera is positioned above the breast and rotated through a range of viewing angles. For each view linear translation stages are used to position the camera as closely as possible to the breast surface. Following reconstruction the resulting 3-D tracer map can then be readily co-registered with the volumetric XBT image.

The objective of this phantom study is to compare image quality in MBIT with that in MBI over a range of radioactivity concentrations in the breast. The image metrics of lesion contrast, lesion signal-to-noise ratio (SNR) and spatial resolution are compared for a range of lesion sizes and depths under conditions of equal total number of detected counts, using a single gamma camera operated in either MBIT mode or MBI mode.

2 Methods

2.1 Experimental Setup

For simplicity rather than using the full DMT system a bench-top setup was constructed to perform the phantom MBIT study. To permit adjustable camera-to-axis of rotation (AOR) separation in addition to varying viewing angle an apparatus was built consisting of a motor-controlled rotation stage mounted on a linear translation stage (Figure 1). In this setup the y-axis is defined to coincide with the AOR, the z-axis is defined to point along the short dimension of the phantom, and the x-axis is defined to result in a right-handed coordinate system. The dose study experiments were done by fabricating gelatin breast phantoms containing spherical simulated lesions. The gamma camera, built at the Jefferson Lab, has a 15 cm × 20 cm field of view and is equipped with a high resolution parallel hole collimator. The overall camera sensitivity is 110.4 cps/MBq (absolute efficiency of 1.1×10^{-4}). The phantom volume was 840 mL, which was the average breast volume of the subjects

participating in our pilot study of DMT [7]. The background activity concentration of the phantoms was 0.33 μCi/mL, corresponding to an injected activity of approximately 25 mCi [8]. As the gelatin hardened as it was refrigerated, hollow, spherical, thin-walled acrylic lesions filled with 10x the background radioactivity concentration (3.3 μCi/mL) were placed in the phantom [2] (see Figure 2). The phantom was contained in a 6.3 cm (z-dimension) x 12 cm (x-dimension) x 7.1 cm (y-dimension) acrylic box to simulate compression to a thickness of 6.3 cm. The box containing the phantom was then mounted on the rotation stage for imaging. The resulting counting rate into the images was approximately 450 cps.

2.2 Image Acquisition

For the study described here 9 evenly spaced views were obtained over 135 degrees. For each view the phantom was positioned as close to the camera as possible, resulting in a maximum camera-to-AOR distance of 13.5 cm (for views 67.5 degrees away from the z-axis) and a minimum camera-to-AOR distance of 6.23 cm (for the view along the z-axis).

In order to evaluate the impact of reduction in injected activity, for each view projection images were obtained over 120 s, 90 s, 60 s, and 30 s to simulate injection of 100%, 75%, 50%, and 25% of the full 25 mCi activity, respectively. Times were adjusted slightly during the course of scanning to take into account radioactive decay. The volumetric MBIT images were reconstructed using an expectation maximization (EM) algorithm developed specifically for MBIT at UVa, which includes resolution recovery and attenuation correction.

In addition to the MBIT projection images, planar MBI images were obtained in which the number of detected counts equaled the total number of counts in the MBIT scans. For example, for the 50% dose acquisition, a 9 minute single-view acquisition time was used for MBI and 9 views x 60 seconds per view for MBIT. For the MBI images the phantom was positioned for viewing along the z-axis and as close as possible to the camera (camera-to-AOR distance of 6.23 cm).

The spatial resolution of planar MBI and MBIT was compared by imaging a point source phantom containing four acrylic posts, each with a 1 mm diameter, 1 mm deep well drilled in its top surface (see Figure 3). A small drop of ^{99m}Tc solution was placed in each well to create four point-like sources in air. MBIT data was obtained using a circular orbit with camera-to-AOR distance of 12.5 cm and 9 views over 135 degrees. The MBI image was taken at 0 degree view. Total acquisition time was 120 seconds for both.

2.3 Image Analysis

Lesion contrast and signal-to-noise ratio (SNR) was calculated for MBIT by constructing regions of interest (ROIs) in the MBIT slices intersecting the lesion centers. Lesion contrast was calculated by taking the mean pixel value of an ROI centered on the lesion and dividing it by the mean pixel value of a nearby background ROI. SNR was calculated by subtracting the mean pixel value of the background ROI from that of the lesion ROI and dividing the result by the standard deviation of the background ROI. Similar ROI analysis was performed on the MBI images. ROI sizes for MBIT analysis and MBI analysis are listed in Tables 1 and 2, respectively. The projection images are 150 × 110 pixels with 1.4 mm × 1.4 mm pixel size and the reconstructed MBIT slices are 94 × 69 with a 2.24 mm × 2.24 mm pixel size.

Spatial resolution was calculated by finding the full width at half maximum (FWHM) of 1-D profiles through the center of the point source images along the x, y, z directions for MBIT and along the y direction for MBI.

3 Results

For the study described here the gelatin phantom contained two each of four sizes of lesion: 1.5 cm, 1.2 cm, 0.9 cm, and 0.76 cm inner diameter. One lesion of each size was placed 1 cm from the side of the phantom closest to the camera (shallow lesions) and the other four lesions were placed 5 cm from the side of the camera closest to the camera (deep lesions).

Figure 4 shows the lesion contrasts and SNR for both MBIT and MBI plotted versus the percent of the current clinical radiotracer dose. Each graph shows the results for a given lesion type (diameter and depth). Error bars signify the standard deviations in 4 repeat trials of nominally identical scans.

Figure 5 compares the spatial resolutions of MBIT and MBI obtained from scans of the point source phantom. For reference, Figure 6 shows the results of a capillary measurement of the gamma camera FWHM spatial resolution over a range of source-to-collimator distances. Given the 12.5 cm AOR-to-detector distance used for the scans of Figure 5, and the fact that the AOR was approximately centered within the phantom, the source-to-collimator distances for the four sources were 8.5, 10.5, 12.5 and 14.5 cm, respectively. Thus the FWHM resolution results for MBI are in substantial agreement with those predicted from the capillary assessment.

4 Discussion

For all lesion sizes and locations tested the contrast and SNR are higher in the images acquired using MBIT compared to those using planar MBI. For both MBIT and MBI there is little change in lesion contrast with changing injected activity. As would be expected, the SNR falls with decreasing total number of image counts for both MBIT and MBI, decreasing by a factor of 1.5 – 2 between activity levels of 100% and 25%. However the superior SNR of MBIT suggests that compared to MBI greater reductions in injected dose might be possible using MBIT. In fact, using only 25% of the activity level as MBI, MBIT has superior contrast and comparable SNR for all lesion sizes and depths.

The spatial resolution in the reconstructed MBIT images is nearly independent of source position within the phantom, unlike that in the MBI images, where resolution is rapidly degraded with increasing source depth. In fact, for all source positions the reconstructed MBIT spatial resolution is substantially superior to that of the gamma camera itself over the range of source-to-collimator separations during the MBIT scan. This fact raises the possibility of utilizing a higher sensitivity collimator which would permit even further reductions in injected activity without unacceptable lesion contrast reduction due to partial volume averaging.

In summary, the contrast, SNR, and spatial resolution of MBIT images were found to be consistently better than those of planar MBI over a range of lesion sizes and locations.

Determination of how much these improvements will ultimately allow the radiation dose to the patient to be reduced before lesion detectability will be unacceptably reduced will require further study. Human studies are needed to evaluate the impact on detectability of inhomogeneous radiotracer distribution in breast tissue. However, these results provide encouragement that MBIT might make substantially lower doses possible than would be possible with planar imaging.

Acknowledgments

This work was supported by the National Institutes of Health (R01 CA149130) and Susan G. Komen for the Cure (KG100479).

References

1. Breast Cancer Statistics. Oct 15. 2011 http://www.breastcancer.org/symptoms/understand_bc/statistics.jsp
2. Maublant J, De Latour M, Mestas D, Clemenson A, Charrier S, Feillel V, Le Bouedec G, Kaufmann P, Dauplat J, Veyre A. Technetium-99m-sestamibi uptake in breast tumor and associated lymph nodes. J Nucl Med. 1996; 37:922–925. [PubMed: 8683312]
3. O'Connor M, Rhodes D, Hruska C. Molecular breast imaging. Expert Review of Anticancer Therapy. 2009; 9:1073–1080. [Review] [37 refs]. [PubMed: 19671027]
4. O'Connor MK, Li H, Rhodes DJ, Hruska CB, Clancy CB, Vetter RJ. Comparison of radiation exposure and associated radiation-induced cancer risks from mammography and molecular imaging of the breast. Med Phys. 2010; 37:6187–6198.
5. Rhodes DJ, Hruska CB, Phillips SW, Whaley DH, O'Connor MK. Dedicated dual-head gamma imaging for breast cancer screening in women with mammographically dense breasts. Radiology. 2011; 258:106–118. [PubMed: 21045179]
6. Wackers FJT, Berman DS, Maddahi J, Watson DD, Beller GA, Stauss HWBCA, Picard M, Holman BL, Fridrich R, Inglese E, Deslaloye B, Bischof-Delaloye A, Camin LMK. Technetium-99m hexakis 2-methoxyisobutyl isonitrile: Human biodistribution, dosimetry, safety, and preliminary comparison to thallium-201 for myocardial perfusion imaging. J Nucl Med. 1989; 30:301–311. [PubMed: 2525610]
7. Williams MB, Judy PG, Gunn S, Majewski S. Dual modality breast tomosynthesis. Radiology. 2010; 255:191–198. [PubMed: 20308457]
8. Williams MB, Narayanan D, More MJ, Goodale PJ, Majewski S, Kieper DA. Analysis of position-dependent compton scatter in scintimammography with mild compression. IEEE Transactions on Nuclear Science. 2003; 50:1643–1649.

Fig. 1.
Gamma camera (top left) and vertical axis rotation stage (lower right), mounted atop the linear translation stage. For clarity the phantom is not shown.

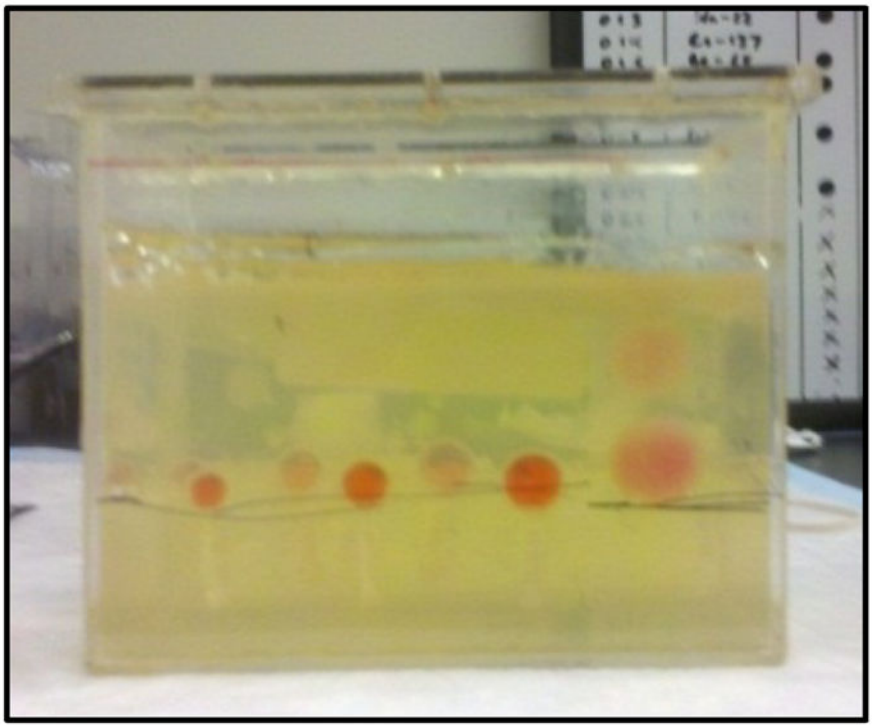

Fig. 2.

Lesion phantom containing a series of simulated lesions with various sizes, placed at two different z locations (depths) within the phantom. In the photo the z-dimension is into the page.

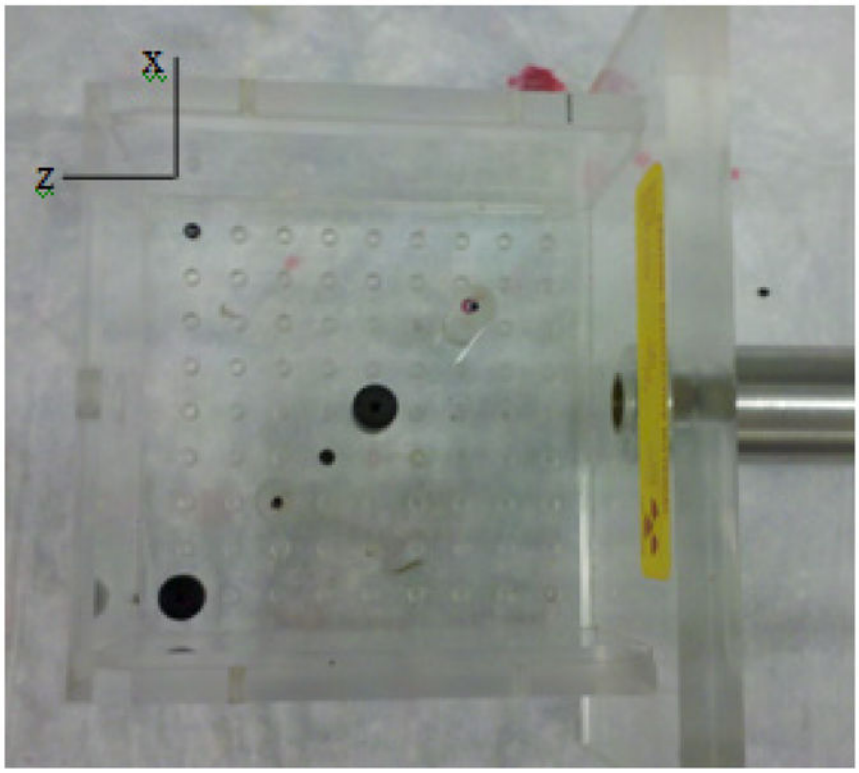

Fig. 3.

Point source phantom. Drops of ^{99m}Tc solution were added to each of four wells of varying heights in y and depths in z and imaged using MBIT and planar MBI

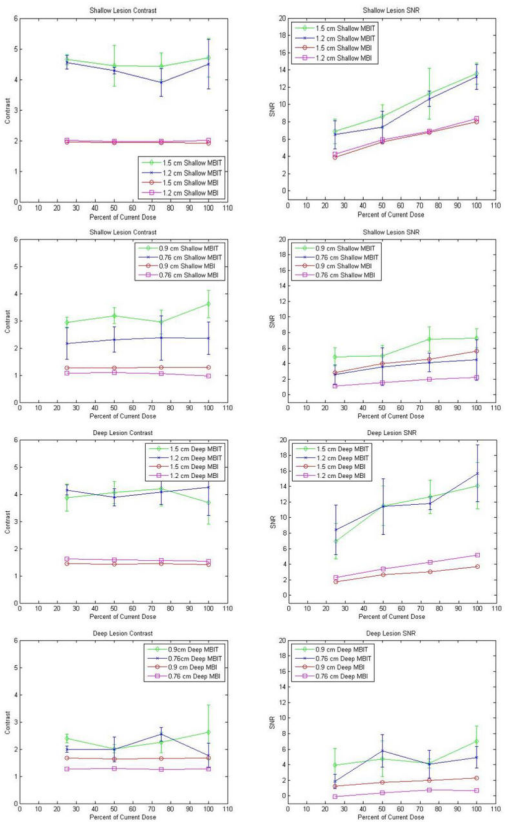

Fig. 4.

Plots of lesion contrast and SNR versus the percent of the current clinical radiotracer dose

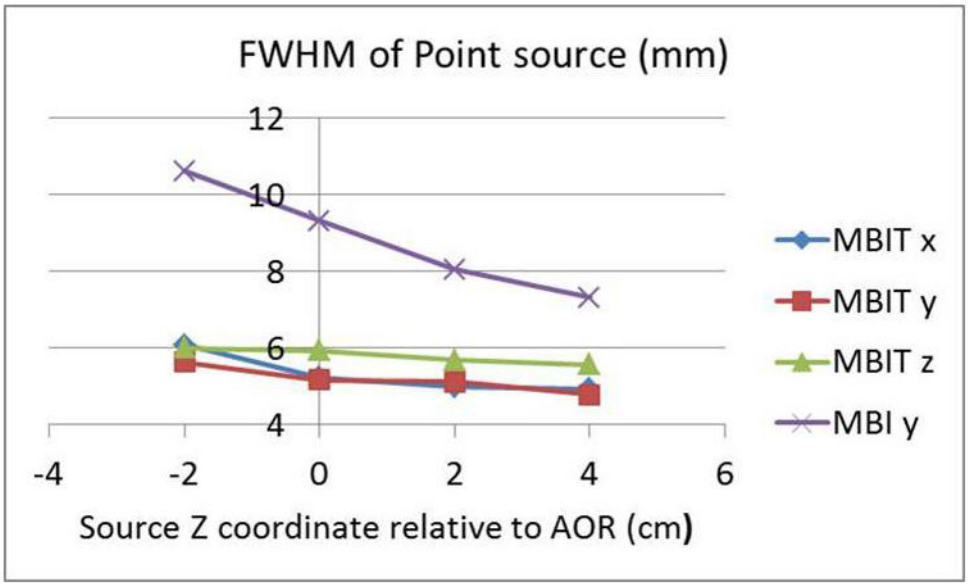

Fig. 5.

Comparison of MBIT and planar MBI spatial resolution. Sources with more positive z-positions are on the camera side of the AOR.

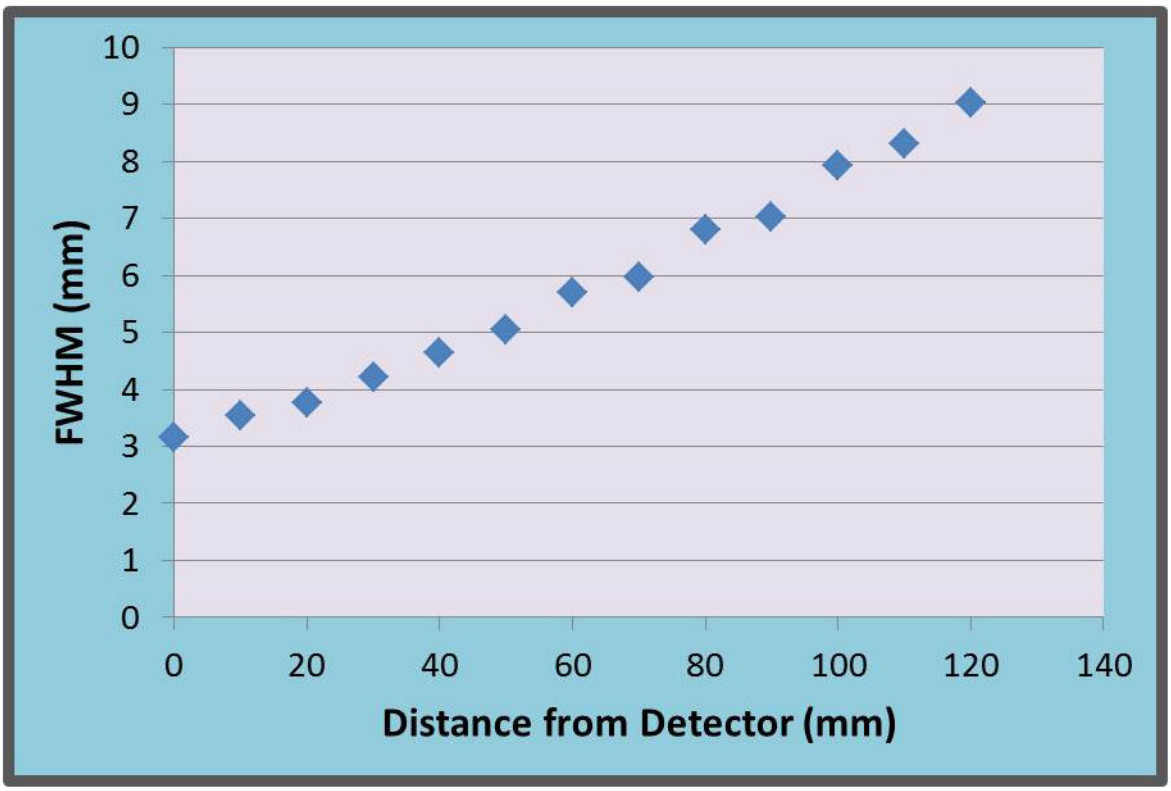

Fig. 6.
Measured gamma camera spatial resolution versus source-to-collimator separation

Table 1

Size of ROIs drawn for MBIT contrast and SNR analysis

Lesion Location	Lesion Inner Diameter	Area of Circular ROI (pixels)
5 cm (Deep)	1.5 cm	16
	1.2 cm	20
	0.9 cm	9
	0.76 cm	9
	Background	416
1 cm (Shallow)	1.5cm	12
	1.2cm	12
	0.9cm	9
	0.76cm	3
	Background	544

Table 2

Size of ROIs drawn for planar MBI contrast and SNR analysis

Lesion Location	Lesion Inner Diameter	Area of Circular ROI (pixels)
5 cm (Deep)	1.5 cm	60
	1.2 cm	44
	0.9 cm	34
	0.76 cm	11
1 cm (Shallow)	1.5 cm	52
	1.2 cm	34
	0.9 cm	31
	0.76 cm	34
	Background	1647